+RESEARCH ARTICLE

Inter-Hemispheric Desynchronization of the Human MT+ during Visually Induced Motion Sickness

Jungo Miyazaki[1], Hiroki Yamamoto[2*], Yoshikatsu Ichimura[1], Hiroyuki Yamashiro[3], Tomokazu Murase[4], Tetsuya Yamamoto[5], Masahiro Umeda[4], Toshihiro Higuchi[6]

1. Corporate R&D, Canon Inc., Tokyo, Japan
2. Graduate School of Human and Environmental Studies, Kyoto University, Kyoto, Japan
3. Department of Medical Engineering, Aino University, Osaka, Japan
4. Department of Medical Informatics, Meiji University of Integrative Medicine, Kyoto, Japan
5. Graduate School of Engineering, Kyoto University, Kyoto, Japan
6. Department of Neurosurgery, Meiji University of Integrative Medicine, Kyoto, Japan

*Correspondence to: **Dr. Hiroki Yamamoto**
Graduate School of Human and Environmental Studies, Kyoto University
YoshidaNihonmatsu-cho, Sakyo-ku, Kyoto 606-8501, Japan
E-mail: yamamoto@cv.jinkan.kyoto-u.ac.jp
Tel: +81-75-753-2978; Fax: +81-75-753-6574

Short Title: Impact of VIMS on the human MT+

Keywords: human visual cortex, optokinetic nystagmus (OKN), vection, functional magnetic resonance imaging (fMRI), visual motion,

ABSTRACT

Visually induced motion sickness (VIMS) is triggered in susceptible individuals by stationary viewing of moving visual scenes. VIMS is often preceded by an illusion of self-motion (vection) and/or by inappropriate optokinetic nystagmus (OKN), responses associated with increased activity in the human motion-sensitive middle temporal area (MT+). Neuroimaging studies have reported predominant right hemispheric activation in MT+ during both vection and OKN, suggesting that VIMS may result from desynchronization of activity between left and right MT+ cortices. However, this possibility has not been directly tested. To this end, we presented VIMS-free and VIMS-inducing movies in that order while measuring the temporal correlations between corresponding left and right visual cortices (including MT+) using functional magnetic resonance imaging (fMRI). The inter-hemispheric correlation was reduced significantly during the viewing of the VIMS-inducing movie compared to the control VIMS-free movie in the MT+ of subjects reporting VIMS, but not in insusceptible subjects. In contrast, there were no significant inter-hemispheric differences within VIMS-free or VIMS-inducing movie exposure for visual area V1, V2, V3, V3A, or V7. Our findings provide the first evidence for an association between asynchronous bilateral MT+ activation and VIMS. Desynchronization of left and right MT+ regions may reflect hemispheric asymmetry in the activities of functional networks involved in eye movement control, vection perception, and/or postural control.

INTRODUCTION

Motion sickness (MS) is a physiological response to certain types of movement, as experienced during sea, air, or space travel. About a third of the population is susceptible to MS (Griffin 1990), although susceptibility varies with gender and age (Golding 2006). The symptoms and signs of MS are classified broadly into the three types: (1) oculomotor disturbances (eyestrain, blurred vision, headache), (2) nausea (stomach awareness, increased salivation, cold sweating, pale skin) and (3) disorientation (dizziness, drowsiness, fatigue) (Shupak & Gordon 2006; Kennedy et al. 2010). These negative effects can last for hours or longer (Kennedy et al. 1993a).

The vestibular system is presumed to play a central role in MS generation since bilateral labyrinthine-defective individuals are immune (Kennedy et al. 1968; Cheung et al. 1991). Several hypotheses have been proposed to explain the physiological basis of MS (see Flanagan et al. 2004 for a review), including the sensory conflict hypothesis (Reason & Brand 1975; Reason 1978; Oman 1990), the eye movement hypothesis (Ebenholtz 1992; Ebenholtz et al. 1994), the subjective vertical conflict theory (Bos & Bles 1998), and the postural instability hypothesis (Riccio & Stoffiregen 1991), all of which include the vestibular system as a key component. However, none of these theories is supported by conclusive evidence.

In addition to actual movement, stationary viewing of a moving visual scene can provoke MS in susceptible observers. This visually induced motion sickness (VIMS) has been reported in a variety of virtual environments (Ellis 1991). Virtual reality has important applications in testing, research, and skill development, so future research on the physiological causes of VIMS could allow for the development of useful virtual applications with reduced risk of VIMS. To address this issue, however, we first need to understand the visual processes that encode the motion signals inducing VIMS. The present study was conducted to examine the possible association of VIMS with specific patterns of activity in visual cortices as revealed by functional magnetic resonance imaging (fMRI).

The putative visual cues for VIMS are explicitly mentioned in two hypotheses for MS, the sensory conflict hypothesis (Reason & Brand 1975; Reason 1978; Oman 1990) and the eye movement hypothesis (Ebenholtz 1992; Ebenholtz et al. 1994). The sensory conflict hypothesis postulates that VIMS results from a conflict or mismatch between motion signals generated by different sensory systems and/or between actual motion signals and expected motion signals stored in sensory memory. In support of this sensory conflict hypothesis, VIMS is often preceded by a compelling illusion of apparent self-motion called vection (Hettinger et al. 1990), which is generally produced by large-field visual motion. Vection may occur when the motion cues provided by visual input and the stationary cues provided by vestibular and/or proprioceptive inputs conflict. On the other hand, the eye movement hypothesis (Ebenholtz 1992; Ebenholtz et al. 1994) postulates that the stretching and/or traction of extraocular muscles induced

by optokinetic nystagmus (OKN), reflexive eye movements produced by moving visual scenes, produce afferent signals that ultimately stimulate the brainstem vomiting center via the vestibular nuclei.

The two cues for VIMS, vection and OKN, are both associated with changing activity within the human motion-sensitive middle temporal area (MT+). During vection, early visual areas and parieto-insular vestibular cortex were deactivated (Brandt et al. 1998; Kleinschmidt et al. 2002), whereas MT+ was either broadly activated (Brandt et al. 1998) or exhibited transient activation associated with shifts in perception (Kleinschmidt et al. 2002). Similarly, OKN was associated with activity in the MT+ as well as V1, frontal eye field, supplementary eye field, ventrolateral premotor cortex, posterior parietal cortex, and cerebellum (Dieterich et al. 1998, 2003; Konen et al. 2006). Notably, hemispheric laterality during both vection and OKN was reported in MT+. Kovacs et al. (2008) reported that the right MT+ was more active during vection than during true object motion while Dieterich et al. (1998) reported prominent right hemispheric activation in the MT+ during OKN.

The close link between these VIMS precursors and right MT+ predominance suggests that divergent activity between left and right MT+ may trigger VIMS. Previous imaging studies could not address this issue because the stimulation periods employed were too short to induce VIMS. Recently, Napadow et al. (2012) measured fMRI activity as subjects viewed translating large stripes for a time sufficient to induce VIMS and found that the subjective feeling of nausea was associated with activation of a broad cortical network including insular and anterior cingulate cortices, but this study did not examine hemispheric laterality.

We hypothesize that VIMS is associated with asymmetric activity in the left and right MT+. This hypothesis was tested by presenting a motion picture acquired by a rapidly moving camera to induce VIMS while measuring the temporal correlation of brain activity in corresponding bilateral cortical regions by fMRI. The present study focused on brain activity directly reflecting visual processing of incoming sensory signals. We isolated this activity component from lower frequency components that reflect functional connectivity between hemispheres by high-pass filtering the fMRI signal (> 0.1 Hz). We predicted that the inter-hemispheric correlation of MT+ activity evoked by the movie would be reduced selectively when subjects experienced VIMS.

METHODS

Subjects

Fourteen healthy adults (12 men, 2 women; mean age 32.9 years, range 25–48 years) with normal or corrected-to-normal vision, including four of the authors, participated in this study. Subjects had no history of psychiatric or neurological disease, and all provided written informed consent to participate. The study protocol was approved by the Human Studies Committee of the Graduate School of Human and Environmental

Studies at Kyoto University and the Department of Neurosurgery at Meiji University of Oriental Medicine.

As described in the Results section, subjects were divided into 2 groups based on their self-reported response to the visual stimuli: a VIMS group (n=8, all men including two authors; age: 32.3 ± 7.2, mean ± *SD*) who reported motion sickness while viewing a VIMS-inducing movie, and a healthy group (n=6, two women and four men including two authors; age: 33.3 ± 7.2, mean ± *SD*) who did not report motion sickness. In addition to group division based on self-reports, a median split criterion, which divided subjects based on the median of the Simulator Sickness Questionnaire (SSQ) score (described below), was employed to separate subjects into groups more objectively.

Visual stimuli

Two motion stimuli were used. The first was a 6-min video clip consisting of three 2-min scenes separated by a 1-s fade-out and fade-in. The scenes were shot with a moving video camera mounted on a hand cart using a special jig consisting of a camera mount and a stepping motor. During image acquisition, the hand cart meandered through a room as the video camera was rotated 60º/s around the axis by the stepping motor, resulting in optical flow consisting of both a translational component due to movement of the hand cart and a rotational component due to the roll of the video camera (Fig. 1A and Online Resource 1). The stimulated area (screen size) subtended 50º by 36º in visual angle. We call this video clip a global motion stimulus since it contained global rotational and translational motion signals. The second motion stimulus, which we call a local motion stimulus, was edited from the global motion stimulus. It was the same size as the first stimulus (50º by 36º) but consisted of 64 panels (in 8 rows and 8 columns), each an identical reduced version of the original video clip (Fig. 1B and Online Resource 2). This movie editing technique was used to equate low-level visual characteristics across stimuli and reduce vection induced by the original global motion stimulus (Wall & Smith 2008), thereby reducing the incidence of VIMS because vection may be a necessary precondition (Hettinger et al. 1990). Thus, the local motion stimulus acted as a control.

The stimuli were projected onto a screen mounted to the top of the subject's head using a digital light processing projector (LVP-HC3800; Mitsubishi, Japan) with a spatial resolution of 1080 × 720 pixels and refresh rate of 60 Hz. Subjects were supine and viewed the stimuli through a planar total reflection mirror at a distance of around 25 cm from the eyes.

-------Figure 1 about here------

Experimental procedure

For each fMRI session, a within-subjects design was used with two stimulus conditions (6 min each) and three intervening resting periods (5 min each). During each resting period, subjects maintained fixation on the center of a gray background projected from the digital projector. After the first resting period, the local motion

stimulus (Fig.1B) was presented, followed in sequence by the second resting period, then the global motion stimulus (Fig.1A), and finally the third resting period. The order of stimulus presentation was not counterbalanced because a preliminary observation suggested that VIMS-susceptible subjects could still be experiencing symptoms during the local motion condition if preceded by the global motion condition.

VIMS severity was assessed before and after each stimulus and resting period (6 times in total) using the Simulator Sickness Questionnaire (SSQ) (Kennedy et al. 1993b). The SSQ consists of 16 items rating the severity of specific symptoms (e.g., eye strain, headache, etc.) on a 4-point scale (none, slight, moderate, and severe). Before and after movie presentations and resting periods, the questionnaire was displayed on the screen and the subjects responded using a 4-button response pad (HH-1x4L; Current Design Inc., Philadelphia, PA). All stimulus presentations were controlled and subject responses were recorded by Presentation software (Neurobehavioral Systems Inc., Albany, CA) on a personal computer (ThinkPad T500; Lenovo, Morrisville, NC).

Brain image acquisition

Functional MR images were acquired on a standard clinical 3-T MRI scanner (Trio TIM; Siemens, Germany) using T2*-weighted gradient-echo echo planer sequence (repetition time [TR] = 2000 ms; echo time [TE] = 30 ms; flip angle [FA] = 90°; voxel size [VS] = 3 × 3 × 4 mm; field of view [FOV] = 192 × 192 mm; 37 slices; axial orientation parallel to the AC-PC plane; interleaved acquisition) with a 20-channel phased-array head coil. The functional volumes were continuously scanned from 10 s before the beginning of the first resting condition until the end of the third resting condition. The total duration of a functional run was about 35 min. To facilitate anatomical registration, structural images were acquired using a 3D magnetization-prepared rapid gradient-echo T1-weighted sequence with following parameters: TR = 1800 ms; TE = 3.03 ms; inversion time [TI] = 650 ms; FA = 9°; VS = 0.8 × 0.8 × 0.8 mm; FOV = 205 × 205 mm; 37 slices; axial orientation parallel to the AC-PC plane; interleaved acquisition. All functional volumes were anatomically registered to a standard structural data set recorded in a separate session, which was also used to reconstruct individual cortical surfaces.

Data analysis

We performed region of interest (ROI) analysis on visual areas V1, V2, V3, V3 accessory (V3A), MT+, and V7. All fMRI data were analyzed with AFNI software (Cox 1996) and in-house software (Yamamoto et al. 2008, 2012). Figure 2 schematically illustrates the procedure for ROI analysis.

ROI definition. After reconstructing each individual's cortical surface from the structural brain volume acquired beforehand, the locations of the retinotopic visual areas were identified individually for each subject by fMRI using multiple retinotopic mapping procedures. The procedures comprised two steps. In the first step, areas V1,

V2, V3, V3A, and V7 were localized using a standard phase-encoding method (Engel et al. 1994; Sereno et al. 1995; De Yoe et al. 1996) with relatively small and thin stimuli (rotating 24° wedge and 2° expanding ring). At this step, area MT+ was only tentatively defined since the MT+ boundaries are somewhat ambiguous owing to the large neuronal receptive fields. Thus, in the second step, we confirmed that the MT+ region included sub-regions MT and MST (medial superior temporal area) as reported in previous studies (e.g. Huk et al. 2002; Smith et al. 2012). This was confirmed using a new phase-encoding stimulus devoid of central visual fields (T. Yamamoto et al. 2009) in conjunction with a standard motion localizer and an ipsilateral motion localizer (Huk et al. 2002). Further details are described in the Online Resource 3 and elsewhere (H. Yamamoto et al. 2008, 2012).

-------Figure 2 about here------

ROI analysis. All fMRI data were first subjected to slice-timing correction and head motion correction. The ROI analysis was then conducted in the following steps: (1) sampling fMRI time series data during each 6-min stimulus condition (180 fMRI volumes per condition), (2) high-pass filtering with a 0.1-Hz cut-off, (3) conversion to percent signal change, (4) removal of outlier voxels showing > 10% signal change, (5) calculation of the average time series for each ROI from non-outlier voxels within the ROI, (6) computation of the inter-hemispheric correlation coefficient between the time-series signals of corresponding left and right ROIs using Pearson's correlation, and (7) Fisher z transformation of the inter-hemispheric correlation to improve normality for statistical analyses. Our use of the relatively high 0.1-Hz cut-off (instead of the more common 0.01-Hz cut-off) was motivated by two factors. Firstly, we were interested in sensory-driven neural activity rather than spontaneous activity. Secondly, prior works have shown that spontaneous activity and fMRI noise have 1/f-like power spectra, with most of the power concentrated below 0.1 Hz (Nir et al. 2008; Bulmore et al. 2001). We confirmed through additional analyses that essentially similar results were obtained with cut-off frequencies lower than 0.1 Hz, including 0.01 Hz (Online Resource 4).

Statistical Analyses

The R package (R Development Core Team 2013) was used for all analyses. A linear mixed-effects model analysis was performed using the function *lmer()* from the *lme4* package in R (Bates, Maechler, Bolker, & Wolter 2013) to evaluate the association between VIMS (as determined by subjective reports and SSQ scores) and the inter-hemispheric synchronization of cortical activity measured by fMRI. For the SSQ total score and three SSQ subscores (nausea, oculomotor, and disorientation) measured after local and global motion stimulus conditions, linear mixed-effects model analyses were conducted with a within-subjects fixed effect CONDITION (local vs. global

motion stimulus condition) and a between-subjects fixed effect GROUP (VIMS group vs. the non-responsive or healthy group). The model also included by-subject random adjustment for the intercept, allowing us to generalize the conclusions from the sample to the population since we can treat subjects as randomly drawn from a population of all potential subjects. To assess inter-hemispheric correlations during both local and global motion conditions, linear mixed-effects model analyses were conducted separately for each visual area ROI with the fixed effects CONDITION and GROUP and random intercepts of subjects.

The significance of the CONDITION × GROUP interaction was assessed by a likelihood-ratio test that compares the models with and without the CONDITION × GROUP interaction term. If there was a significant CONDITION × GROUP interaction, *p* values are reported for only the interaction because the significance of the main effect is uninterpretable (Zar 1999). In these cases, the simple effect of CONDITION is reported instead as yielded by the function *testInteractions()* from the *phia* package in R (Rosario-Martinez, Fox, & R Core Team 2013). If there was no significant interaction, the main effect of CONDITION was evaluated by a likelihood-ratio test comparing models with and without the CONDITION term. For each main and simple effect, a pseudo R^2 was calculated in order to quantify the effect size according to (1)

$$R^2 = 1 - \exp\left\{-\frac{2}{n}\left(L_m - L_0\right)\right\} \quad (1)$$

where n is the number of observations, and L_m and L_0 are the log-likelihood of the models with and without the target variable, respectively.

For testing the relationship between the inter-hemispheric correlation and SSQ score, Kendall rank correlation coefficient (τ) was calculated and the statistical significance was evaluated by the function *Kendall*() from the *Kendall* package in R.

The significance level for all statistical tests was 0.05. The reported *p* values for the interaction, simple effect, and main effect were Bonferroni-corrected to account for multiple comparisons across SSQ scores, visual area ROIs, and groups.

RESULTS

Visually induced motion sickness

Eight of the 14 subjects (all men) stated that they felt motion sick while viewing the global motion video (Fig. 1A, the global motion condition) but not while viewing the local motion video (Fig. 1B, the local motion condition). The remaining 6 subjects

reported no VIMS under either condition. The 8 subjects reporting VIMS were classified as the VIMS group and the other 6 subjects as the healthy group. The relationships between individual subjective reports and SSQ scores are shown in Figure 3. The rank order of the individual subject total SSQ scores was consistent with the group classification, and the two groups were clearly separated by a cut-off total score around 20, which corresponds to the SSQ score empirically proposed for VIMS diagnosis (Kennedy et al. 1993b).

-------Figure 3 about here------

Figure 4A compares the total SSQ scores between the VIMS and healthy group at the 6 SSQ test points during the experimental session. In the VIMS group, the mean SSQ total score was markedly higher after the global motion condition compared to the local motion condition, while the mean total SSQ score of the healthy group remained near baseline throughout the experimental session. Similar results were obtained for the SSQ subscores nausea, oculomotor, and disorientation (Figure 4B). These results were analyzed by a repeated-measures linear mixed-effects model including the fixed effects CONDITION (local vs. global motion condition) and GROUP (VIMS vs. healthy group), and the random effect of subject (Table 1). For the SSQ total score, there was a significant CONDITION × GROUP interaction ($\chi^2(1) = 8.45$, $p = 0.015$, Bonferroni corrected). Post hoc tests for the simple effect of CONDITION showed a significant increase in SSQ total score between local and global motion conditions only for the VIMS group (VIMS: $\chi^2(1) = 28.71$, $p < 0.001$; healthy: $\chi^2(1) = 0.03$, $p > 1$, Bonferroni corrected). Similar results were obtained for the SSQ subscores (oculomotor: CONDITION × GROUP interaction: $\chi^2(1) = 7.87$, $p = 0.02$; the simple effect of CONDITION: VIMS: $\chi^2(1) = 29.91$, $p < 0.001$; healthy: $\chi^2(1) = 0.19$, $p > 1$; disorientation: CONDITION × GROUP interaction: $\chi^2(1) = 10.46$, $p = 0.004$; the simple effect of CONDITION: VIMS: $\chi^2(1) = 29.20$, $p < 0.001$; healthy: $\chi^2(1) = 0$, $p > 1$, Bonferroni corrected), except nausea (CONDITION × GROUP interaction: $\chi^2(1) = 4.91$, $p = 0.107$; the main effect of CONDITION: $\chi^2(1) = 5.53$, $p = 0.075$, Bonferroni corrected).

-------Figure 4 about here------

-------Table 1 about here------

Inter-hemispheric MT+ desynchronization during visually induced motion sickness

To test our hypothesis that left and right MT+ activities desynchronize during VIMS, we compared the inter-hemispheric correlation of fMRI signals from MT+ and other visual areas (V1, V2, V3, V3A, and V7) between the local and the global motion

conditions (Figure 5). For all 8 VIMS subjects, the inter-hemispheric temporal correlation of MT+ signals decreased from the local to the global motion condition (Fig. 5A) as predicted by the hypothesis, whereas the change in inter-hemispheric correlation between conditions showed no consistent pattern for the 6 healthy subjects (Fig. 5D). A decrease in the inter-hemispheric correlation between the local and global motion condition was also observed in V1 for all VIMS subjects except one (Fig. 5B), but again there was no consistent change among the healthy subjects (Fig. 5E).

-------Figure 5 about here------

The mean inter-hemispheric correlation coefficient for MT+ was significantly lower in the VIMS group while viewing the global motion video compared to the local motion video (Figure 6A). In contrast, the mean inter-hemispheric correlation coefficient did not differ between conditions for the healthy group. The mean inter-hemispheric correlation coefficient for V1 was also lower in the VIMS group while viewing the global motion video compared to the local motion video, but the difference did not reach statistical significance (Fig. 6B).

-------Figure 6 about here------

As in the analysis of SSQ scores (Table 1), a linear mixed-effects model including the fixed effects CONDITION (local vs. global motion condition) and GROUP (VIMS vs. healthy group), and the random effect of subject was used to compare inter-hemispheric activity correlations for corresponding ROIs between conditions and groups (Table 2). For MT+, there was a significant CONDITION × GROUP interaction (χ^2 (1) = 11.66, p = 0.004, Bonferroni corrected). Post hoc tests for the simple effect of CONDITION showed that the inter-hemispheric correlation of MT+ activity decreased significantly in the VIMS group during the global motion condition compared to the local motion condition ($\chi^2(1) = 28.71$, $p < 0.001$, Bonferroni corrected), whereas there was no significant change in inter-hemispheric correlation of MT+ activity for the healthy group between conditions ($\chi^2(1) = 3.47$, $p = 0.751$, Bonferroni corrected). For V1, the interaction effect was not significant ($\chi^2(1) = 4.92$, $p = 0.159$, Bonferroni corrected) and the VIMS-specific decrease in inter-hemispheric correlation was non-significant ($\chi^2(1) = 6.59$, $p = 0.062$, Bonferroni corrected). For the other visual areas V2, V3, V3A, and V7, there was no significant interaction between CONDITION and GROUP (V2: $\chi^2(1) = 1.74$, $p > 1$; V3: $\chi^2(1) = 2.78$, $p = 0.573$; V3A: $\chi^2(1) = 0.45$, $p > 1$; V7: $\chi^2(1) = 5.04$, $p = 0.149$, Bonferroni corrected), and no significant change in inter-hemispheric

correlation from the local to global motion condition (V2: $\chi^2(1) = 5.19$, $p = 0.137$; V3: $\chi^2(1) = 1.86$, $p > 1$; V3A: $\chi^2(1) = 0.05$, $p > 1$; V7: $\chi^2(1) = 0.02$, $p > 1$, Bonferroni corrected). The above results were replicated using the median split criterion, in which subjects were divided into seven healthy group members and seven VIMS group members based on the median SSQ total score (see Online Resource 5). In sum, the inter-hemispheric correlation of left and right MT+ activities decreased during VIMS, whereas other visual areas did not show such inter-hemispheric asymmetry in activity during VIMS.

-------Table 2 about here------

Correlation analysis

Can we predict the degree of motion sickness from the inter-hemispheric correlation? To answer this, we examined whether the severity of motion sickness can be predicted from the degree of inter-hemispheric MT+ activity desynchronization. To this end, we determined the change in inter-hemispheric correlation and the change in SSQ total score from local to global motion conditions (global - local), and then computed the Kendall rank correlation between the two changes for each visual area. The rank correlation showed a non-significant negative trend for MT+ and V1 (MT+: $\tau = -0.54$, $p = 0.057$; V1: $\tau = -0.54$, $p = 0.057$, Bonferroni-corrected), indicating that the greater the decrease in inter-hemispheric correlation from the local to global motion condition (greater desynchronization), the higher the SSQ total score (Figure 7). For other areas, the rank correlation was not significant (V2: $\tau = -0.33$, $p = 0.656$; V3: $\tau = -0.50$, $p = 0.106$; V3A: $\tau = -0.18$, $p > 1$; V7: $\tau = -0.45$, $p = 0.188$, Bonferroni-corrected).

-------Figure 7 about here------

DISCUSSION

We hypothesized that VIMS would differentially affect the neural responses in left and right MT+, and tested this by acquiring fMRI signal time series from multiple visual cortical regions, including MT+, while subjects viewed VIMS-free and VIMS-inducing videos. The inter-hemispheric temporal correlation of MT+ activity decreased significantly during VIMS. A decrease was also observed for V1 but the effect was not as robust as in MT+, and there were no effects of VIMS on inter-hemispheric correlations in the other extrastriate areas examined, V2, V3, V3A, and V7. Moreover, correlation analysis suggested the possibility of predicting the subjective severity of motion sickness from the inter-hemispheric correlation of MT+.

To our knowledge, this is the first report demonstrating an association between VIMS and asymmetric activation of left and right MT+ regions, although the sample-size here was relatively small.

Compared to model-based approaches for fMRI analysis, time series correlation analysis of fMRI data offers an unbiased method for revealing unexpected changes in cortical activity associated with various neurological conditions. In contrast to our results, Napadow et al. (2012) identified a VIMS-related network broadly distributed over interoceptive, limbic, and somatosensory regions, but found no association between VIMS and visual cortex. Presumably, the effects of VIMS on the temporal characteristics of activity in visual cortices were more complex than assumed in that study. Alternatively, inter-hemispheric correlation analysis can detect such unpredictable effects since the analysis makes no assumptions about the temporal characteristics of the BOLD signal. Indeed, Hasson et al. (2009) found reduced inter-subject correlations among multiple fMRI time series in autistic subjects compared to healthy controls while watching the same popular movie, underscoring the power of inter-hemispheric and inter-subject correlation analyses to detect unpredictable changes in brain activity as may occur in neurological diseases.

All subjects in the VIMS-resistant healthy group exhibited high inter-hemispheric correlations in visual cortex during both the local and global motion stimuli. Similar results were also obtained for the VIMS group in most visual cortical regions, except for MT+ during VIMS induced by global motion. High inter-hemispheric correlation is expected from the retinotopic organization of the visual areas and the stimulus configurations. The local motion stimulus would elicit similar responses in left and right visual areas because the right and left halves of the stimulus were comprised of a mosaic of identical frames depicting the same local motion. Similarly, although the two sides of the global motion stimulus were not identical, they had similar local and global motion components, so again it is not surprising that most bilateral visual areas showed relatively high activity correlations.

Why then did MT+ not maintain high temporal correlation between hemispheres during VIMS? It seems unlikely that the effect can be explained by side effects of VIMS such as fatigue, reduced arousal, or disrupted attention, effects that would alter activity in many visual areas. Moreover, desynchronization was observed selectively in MT+, a region responsible for encoding visual motion, which is the very cause of VIMS. It is therefore more plausible that inter-hemispheric desynchronization of MT+ activity reflects hemispheric asymmetry within functional networks related to the incidence of VIMS.

The relevant networks and processes are a matter of conjecture. One possibility is the network related to optokinetic nystagmus (OKN), a principal component of the eye movement hypothesis of MS (Ebenholtz 1992; Ebenholtz et al. 1994). As laterality of MT+ activity with right dominance was reported during OKN (Dieterich et al. 1998), right MT+ activity may reflect or cause aberrant behavior of the eye movement control

system during the global motion stimulus, leading to unusual stretching and/or traction of extraocular muscles in both eyes. Consequently, the afferent signals generated by extraocular muscles may stimulate the area postrema and vagus nerve, resulting in the symptoms of VIMS.

The second possibility is a network related to vection activated by sensory conflict (Reason & Brand 1975, Reason 1978; Oman 1990). The right MT+ was found to be more active during vection than during real object motion (Kovacs et al. 2008), suggesting that MT+ activation is involved in networks associated with the generation of vection. Although the precise mechanism remains unclear, the right dominance of MT+ suggests distinct roles for right and left MT+ in networks integrating sensory information to detect mismatches.

The third possibility is that desynchronization of MT+ activity may be caused by interactions within sensory integration networks. There are at least two possible interactions. One is with the anterior insular cortex, which is thought to play an important role in monitoring activity in the sensory cortex that could lead to disturbances of homeostasis (Sterzer & Kleinschmidt 2010). In the course of VIMS, fMRI activity in right fronto-insular cortex (including the anterior insula) was correlated with the severity of nausea (Napadow et al. 2012), and the white matter tract connecting the right insular cortex and right MT+ was associated with VIMS susceptibility (Napadow et al. 2013). Another possible interaction is with the parieto-insular vestibular cortex. According to sensory conflict theory (Reason & Brand 1975; Reason 1978; Oman 1990), motion sickness can arise from a conflict or mismatch between motion signals generated by different sensory systems, including visual-vestibular conflict, suggesting some form of interaction between the visual and vestibular cortices. Brandt et al. (1998) proposed a reciprocal inhibitory interaction between these systems based on observed reciprocal activation-deactivation patterns. We speculate that the right and left MT+ regions are differentially modulated by these visual-vestibular interactions or are uniquely involved in these networks, leading to inter-hemispheric desynchronization.

Acknowledgement

We thank Dr. Yoshimichi Ejima and Shigeko Takahashi for their helpful comments. We also thank anonymous reviewers for their constructive comments and suggestions. This study was supported by a Grant-in-Aid for Scientific Research on Innovative Areas "Shitsukan" (23135517, 25135720) from the Ministry of Education, Culture, Sports, Science and Technology of Japan and Grants-in-Aid for Scientific Research (22530793) from the Japan Society for the Promotion of Science (JSPS) to H. Yamamoto. The final publication is available at Springer via http://dx.doi.org/10.1007/s00221-015-4312-y

REFERENCES

Bos JE, Bles W (1998) Modelling motion sickness and subjective vertical mismatch detailed for vertical motions. Brain Res Bull. 47(5), 537-542.

Brandt T, Bartenstein P, Janek A, Dieterich M (1998) Reciprocal inhibitory visual-vestibular interaction. Visual motion stimulation deactivates the parieto-insular vestibular cortex. Brain 121(Pt 9): 1749-1758.

Bullmore E, Long C, Suckling J, Fadili J, Calvert G, Zelaya F, Brammer M (2001) Colored noise and computational inference in neurophysiological (fMRI) time series analysis: resampling methods in time and wavelet domains. Human brain mapping 12(2) 61-78.

Cheung BSK, Howard IP, Money KE (1991) Visually-induced sickness in normal and bilateral labyrinthine-defective subjects. Aviat Space Environ Med. 62: 527-531.

Cox RW (1996) AFNI: software for analysis and visualization of functional magnetic resonance neuroimages. Comput Biomed Res. 29: 162-173.

De Yoe EA, Carman GJ, Bandettini P, Glickman S, Wieser J, Cox R, Miller D, Neitz J (1996) Mapping striate and extrastriate visual areas in human cerebral cortex. Proc Nat Acad Sci. (USA) 93: 2382-2386.

Dieterich M, Bucher SF, Seelos KC, Brandt T (1998). Horizontal or vertical optokinetic stimulation activates visual motion-sensitive, ocular motor and vestibular cortex areas with right hemispheric dominance. An fMRI study. Brain 121(8), 1479-1495.

Dieterich M, Bense S, Stephan T, Yousry TA, Brandt T (2003). fMRI signal increases and decreases in cortical areas during small-field optokinetic stimulation and central fixation. Exp Brain Res. 148(1), 117-127.

Ebenholtz S (1992) Motion sickness and oculomotor systems in virtual environments. Presence: Teleoperators and Virtual Environments. 1:3, 302-305.

Ebenholtz SM, Cohen MM, Linder BJ (1994) The possible role of nystagmus in motion sickness: a hypothesis. Aviat Space Environ Med. 65(11), 1032-1035.

Ellis SR (1991) Nature and origins of virtual environments: A bibliographical essay. Comput Syst Eng. 2(4), 321-347.

Engel SA, Rumelhart DE, Wandell BA, Lee AT, Glover GH, Chichilnisky EJ, Shadlen MN (1994) fMRI of human visual cortex. Nature 369: 525.

Flanagan MB, May JG, Dobie TG. (2003) The role of vection, eye movements and postural instability in the etiology of motion sickness. J Vestib Res. 14(4), 335-346.

Golding JF (2006) Motion sickness susceptibility. Auton Neurosci. 129(1), 67-76.

Griffin MJ (1990) Handbook of human vibration. Academic press.

Hasson U, Avidan G, Gelbard H (2009) Shared and idiosyncratic cortical activation patterns in autism revealed under continuous real-life viewing conditions. Autism Res. 2: 220-231.

Hettinger LJ, Berbaum KS, Kennedy RS, Dunlap WP, Nolan MD (1990) Vection and simulator sickness. Mil Psychol. 2(3):171-81.

Huk AC, Dougherty RF, Heeger DJ (2002) Retinotopy and functional subdivision of human areas MT and MST. J Neurosci, 22(16), 7195-7205.

Kennedy RS, Graybiel A, McDonough RC, Beekwith FD (1968) Symptomatology under storm conditions in the North Atlantic in control subjects and in persons with bilateral labyrinthine defects. Acta-Oto-Laryngologica 66: 533-540.

Kennedy RS, Fowlkes J, Lilienthal M (1993a) Postural and performance changes following exposures to flight simulators. Aviat Space Environ Med. 64:10, 912 - 920.

Kennedy RS, Lane NE, Berbaum KS, Lilienthal MG (1993b) Simulator sickness questionnaire: an enhanced method for quantifying simulator sickness. Int J Aviat Psychol. 3(3): 203-220.

Kennedy RS, Drexler J, Kennedy RC (2010) Research in visually induced motion sickness. Appl Ergon. 41(4): 494-503.

Konen CS, Kleiser R, Seitz RJ, Bremmer, F (2005) An fMRI study of optokinetic nystagmus and smooth-pursuit eye movements in humans. Exp Brain Res. 165(2), 203-216.

Kovacs G, Raabe1 M, Greenlee MW (2008) Neural correlates of visually induced self-motion illusion in depth. Cereb Cortex 18 (8): 1779-1787.

Napadow V, Li A, Loggia ML, Kim J, Schalock PC, Lerner E, Tran TN, Ring J, Rosen BR, Kaptchuk TJ, Pfab F (2012) The brain circuitry underlying the temporal evolution of nausea in humans. Cereb Cortex. 23(4): 806-813.

Napadow V, Sheehan J, Kim J, Dassatti A, Thurler AH, Surjanhata B, Vangel M, Makris N, Schaechter JD, Kuo B (2013) Brain white matter microstructure is associated with susceptibility to motion-induced nausea. Neurogastroenterol Motil. 25(5):448-e303

Nir Y, Mukamel R, Dinstein I, Privman E, Harel M, Fisch L, Malach R (2008) Interhemispheric correlations of slow spontaneous neuronal fluctuations revealed in human sensory cortex. Nature neuroscience 11(9) 1100-1108.

Oman CM (1990) Motion sickness: A synthesis and evaluation of the sensory conflict theory. Can J Physiol Pharmacol. 68(2), 294-303

Reason JT, Brand JJ (1975) Motion sickness. London Academic Press.

Reason JT (1978) Motion sickness adaptation: A neural mismatch model. Journal of the Royal Society of Medicine, 71(11), 819-829.

Sereno MI, Dale AM, Reppas JB, Kwong KK, Belliveau JW, Brady TJ, Rosen BR, Tootell RB (1995) Borders of multiple visual areas in humans revealed by functional magnetic resonance imaging. Science 268: 889-893.

Smith AT, Wall MB, Thilo KV (2012) Vestibular inputs to human motion-sensitive visual cortex. Cereb Cortex 22(5), 1068-77.

Sterzer P, Kleinschmidt A (2010) Anterior insula activations in perceptual paradigms: often observed but barely understood. Brain Struct Funct. 214(5-6): 611-22.

Shupak A, Gordon CR (2006). Motion sickness: advances in pathogenesis, prediction, prevention, and treatment. Aviat Space Environmen Med. 77(12), 1213-1223.

Wall MB, Smith AT (2008) The representation of egomotion in the human brain. Curr Biol. 18: 191-194.

Yamamoto H, Ban H, Fukunaga M, Umeda M, Tanaka C, Ejima Y (2008) Large- and small-scale functional organization of visual field representation in the human visual cortex. In: Visual Cortex: New Research, edited by Portocello TA, Velloti RB. New York: Nova Science Publisher, 195-226.

Yamamoto H, Fukunaga M, Takahashi S, Mano H, Tanaka C, Umeda M, Ejima Y (2012) Inconsistency and uncertainty of the human visual area loci following surface-based registration: probability and entropy maps. Hum Brain Mapp. 33: 121-129.

Yamamoto T, Yamamoto H, Mano H, Umeda M, Tanaka C, Kawano K (2009) A new fMRI method for subdividing the human middle temporal complex into retinotopic areas. Neuroscience Research 65, S173.

Table 1. Summary statistics for linear mixed-effects model analysis of SSQ scores
The results of the linear mixed-effects model analysis with the fixed effects CONDITION (local vs. global motion) and GROUP (VIMS vs. healthy) for Simulator Sickness Questionnaire (SSQ) scores. If there was a significant interaction, a post hoc test was conducted for the simple effect of CONDITION. The effect size for the simple effect is a pseudo R2, indicating the goodness of fit of the model with the CONDITION term. If there was no significant interaction, the main effect of CONDITION was examined. Both the interaction and the main effect p values are Bonferroni-corrected for multiple comparisons among the four SSQ scales (total and three subscores), and the post hoc simple effect p values are corrected for multiple comparisons between the two subject groups (VIMS and healthy).

Parameter	Scale	CONDITION × GROUP interaction		Simple effect of CONDITION						Main effect of CONDITION		
		coefficient estimate ± standard error	**statistics** p value (χ^2)	**coefficient** estimate ± standard error		**statistics** p value (χ^2)		**Effect size** R^2		**coefficient** estimate ± standard error	**statistics** p value (χ^2)	**Effect size** R^2
				VIMS	**Healthy**	**VIMS**	**Healthy**	**VIMS**	**Healthy**			
SSQ score	Total score	44.88 ± 13.33	.015 (8.43)	46.75 ± 11.45	1.87 ± 1.92	< .001 (28.71)	> 1 (0.03)	0.47	0.07	N/A	N/A	N/A
	Nausea	40.15 ± 16.56	.107 (4.91)	N/A		N/A		N/A		24.53 ± 9.77	.075 (5.53)	0.17
	Oculomotor	24.95 ± 7.68	.020 (7.87)	27.48 ± 6.28	2.53 ± 2.92	< .001 (29.91)	> 1 (0.19)	0.46	0.06	N/A	N/A	N/A
	Disorientation	62.64 ± 17.71	.004 (10.46)	62.64 ± 14.87	0.00 ± 3.28	< .001 (29.20)	> 1 (0)	0.53	0	N/A	N/A	N/A

Table 2. Summary statistics for linear mixed-effects model analysis of regional inter-hemispheric time series correlations
The results of the linear mixed-effects model analysis with the fixed effects CONDITION (local vs. global motion) and GROUP (VIMS vs. healthy groups) for the inter-hemispheric correlation of visual cortical areas MT+, V1, V2, V3, V3A, and V7. Since there was a significant interaction for MT+, a post hoc test was conducted for the simple effect of CONDITION. The effect size for the simple effect is a pseudo R2, indicating the goodness of fit of the model with the CONDITION term. By contrast, there were no significant interactions for other visual areas. The main effect of CONDITION was thus examined. Both the interaction and the main effect p values are Bonferroni-corrected for multiple comparisons between the six pairs of visual areas, and the post hoc simple effect p values are corrected for multiple comparisons between subject groups.

Parameter	Visual area	CONDITION × GROUP interaction		Simple effect of CONDITION						Main effect of CONDITION		
		coefficient estimate ± standard error	**statistics** p value (χ^2)	**coefficient** estimate ± standard error		**statistics** p value (χ^2)		**Effect size** R^2		**coefficient** estimate ± standard error	**statistics** p value (χ^2)	**Effect size** R^2
				VIMS	**Healthy**	**VIMS**	**Healthy**	**VIMS**	**Healthy**			
Inter-hemispheric correlation	MT+	−0.30 ± 0.07	.004 (11.66)	−0.20 ± 0.02	0.10 ± 0.08	< .001 (28.71)	.751 (3.47)	0.77	0.11	N/A	N/A	N/A
	V1	−0.32 ± 0.13	.159 (4.92)	N/A		N/A		N/A		−0.22 ± 0.08	.062 (6.59)	0.21
	V2	−0.16 ± 0.11	> 1 (1.74)	N/A		N/A		N/A		−0.15 ± 0.06	.137 (5.19)	0.17
	V3	−0.21 ± 0.12	.573 (2.78)	N/A		N/A		N/A		−0.09 ± 0.07	> 1 (1.86)	0.06
	V3A	−0.08 ± 0.13	> 1 (0.45)	N/A		N/A		N/A		−0.01 ± 0.06	> 1 (0.05)	< 0.01
	V7	−0.23 ± 0.09	.149 (5.04)	N/A		N/A		N/A		0.01 ± 0.06	> 1 (0.02)	< 0.01

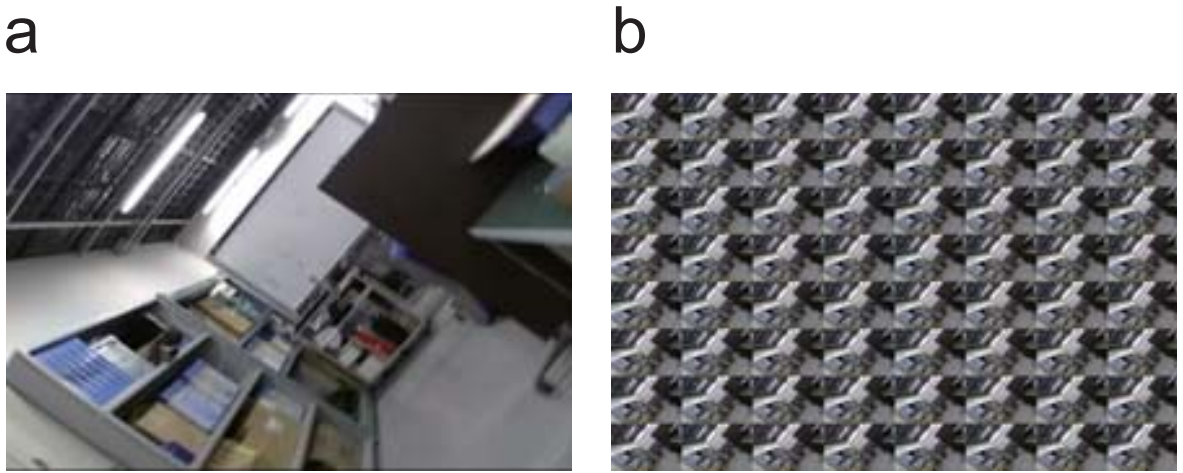

Figure 1. The visual stimuli. (a) A sample frame from the video clip used in the global motion condition. A camera mounted on a cart with a swivel axis is subjected to both translational and rotational motion. (b) A sample frame used in the local motion condition.

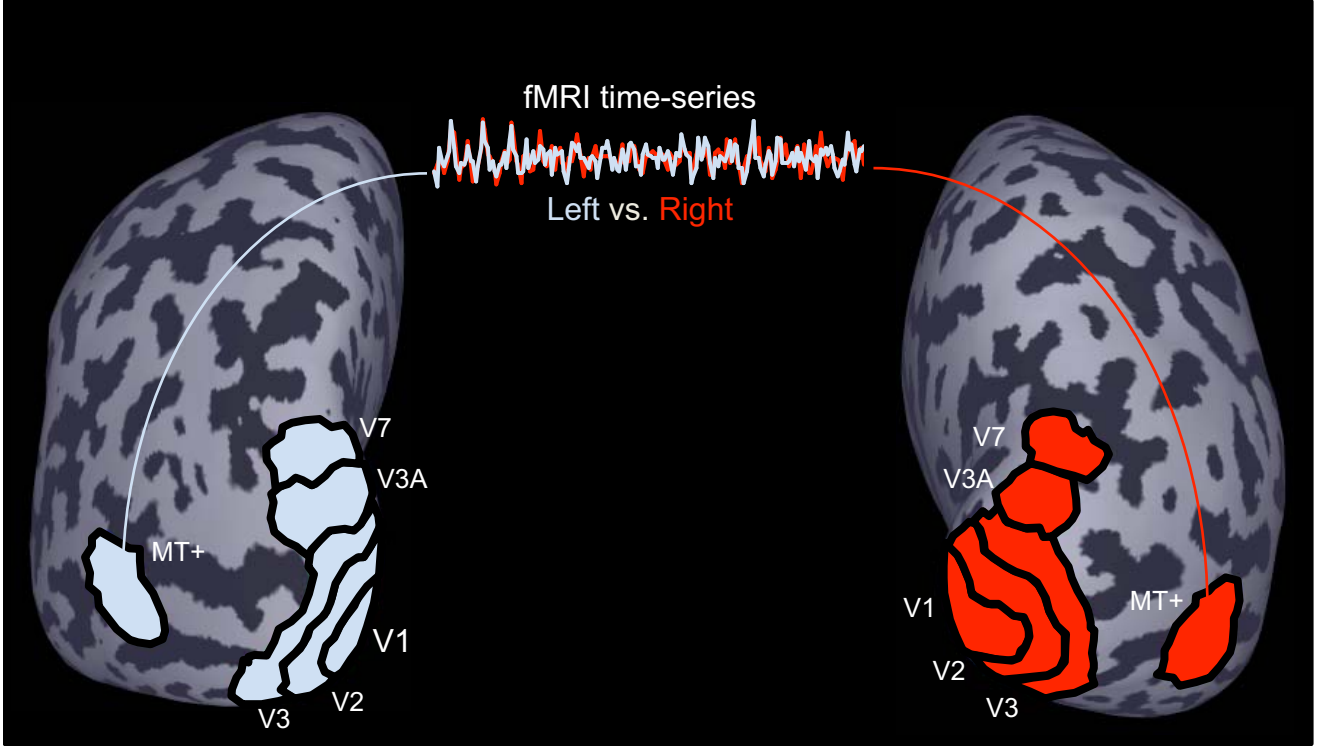

Figure 2. A schematic of the analyses used to investigate inter-hemispheric temporal activity correlations in the human visual cortex. Left and right panels are posterior views of the left and right inflated cortical surfaces, respectively. The six visual areas investigated (V1, V2, V3, V3A, V7, and MT+) are colored (blue: left areas, red: right areas). For each visual area, the functional magnetic resonance imaging time series was averaged across all non-outlier voxels within the area and Pearson correlation coefficients calculated for corresponding time series (blue and red lines in the middle panel).

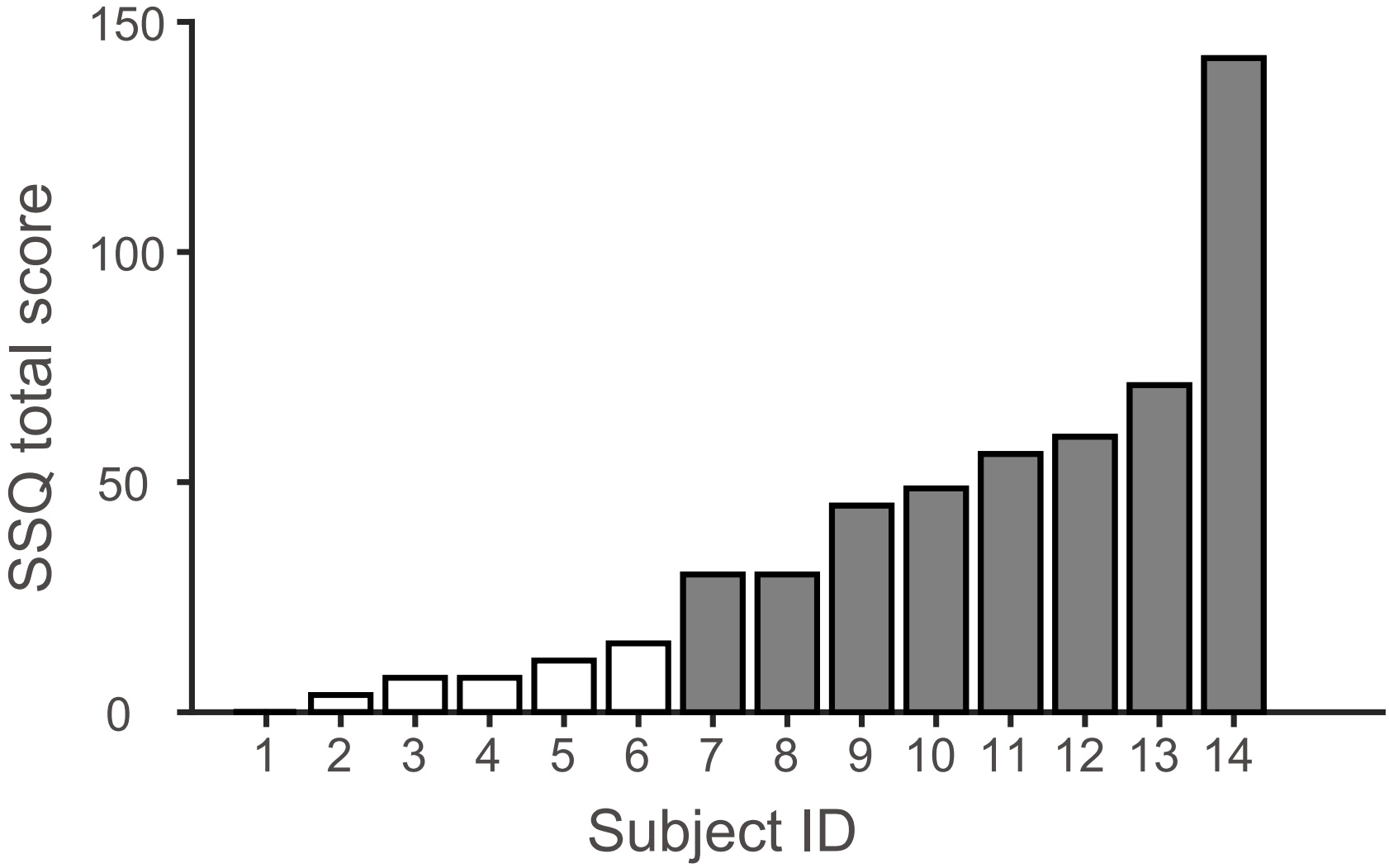

Figure 3. Individual Simulator Sickness Questionnaire (SSQ) total scores measured after the global motion condition. Gray bars indicate the scores of the subjects who self-reported motion sickness after the experimental session (visually induced motion sickness [VIMS] group) and white bars indicate scores of subjects who did not (healthy group).

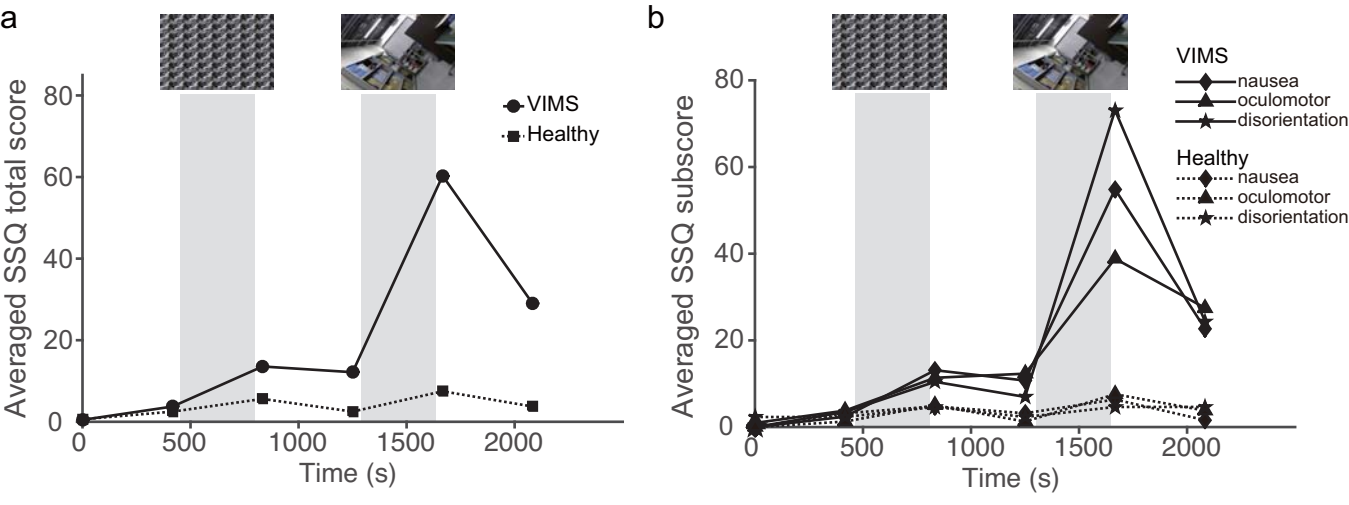

Figure 4. SSQ scores and subscores over the time course of the experimental session. The scores were averaged among subjects in the VIMS group (solid lines) and in the healthy group (dotted lines). The left gray bar indicates the presentation period of the local motion stimulus and the right bar the period of the global motion stimulus (as denoted by the image icons above the bars). (a) SSQ total score. (b) SSQ subscores for nausea, oculomotor, and disorientation.

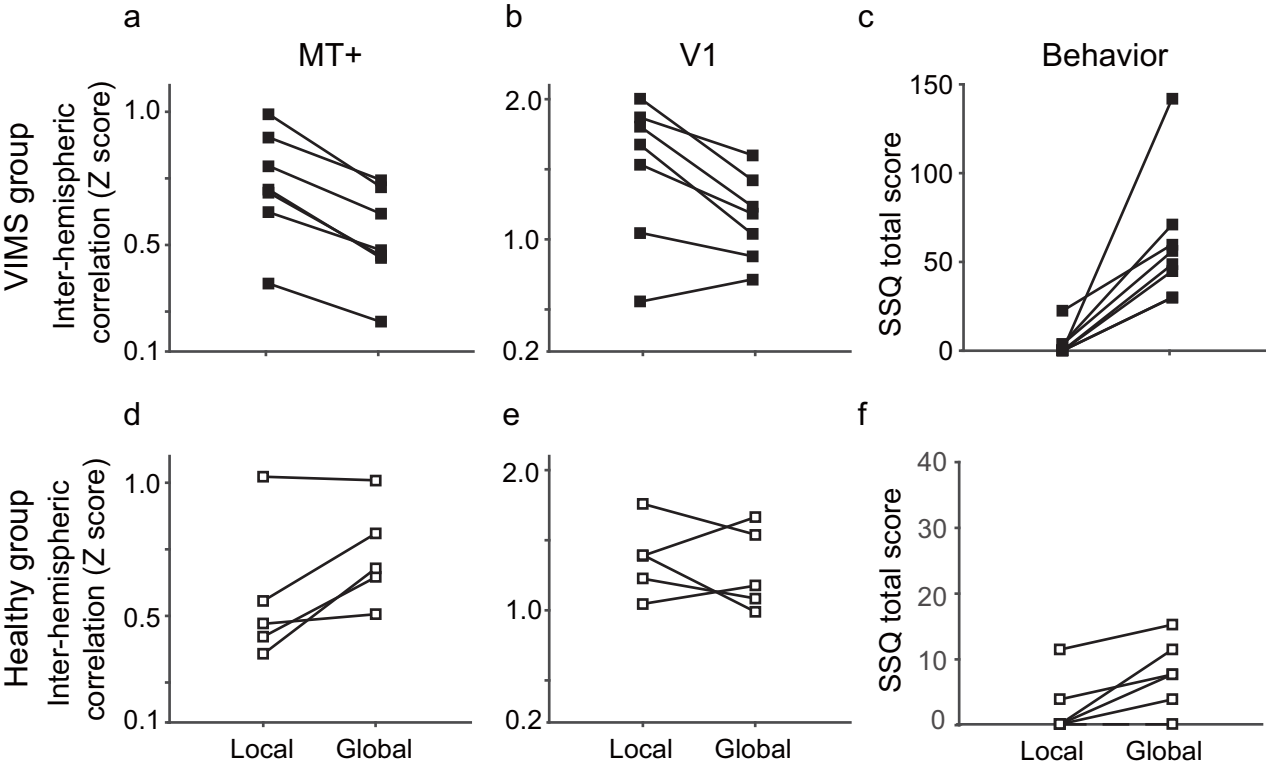

Figure 5. Comparison of individual inter-hemispheric correlations and SSQ scores between the local and the global motion conditions for the VIMS group (a-c) and the healthy group (d-f). Time series are from MT+ (a, d) and V1 (b, e).

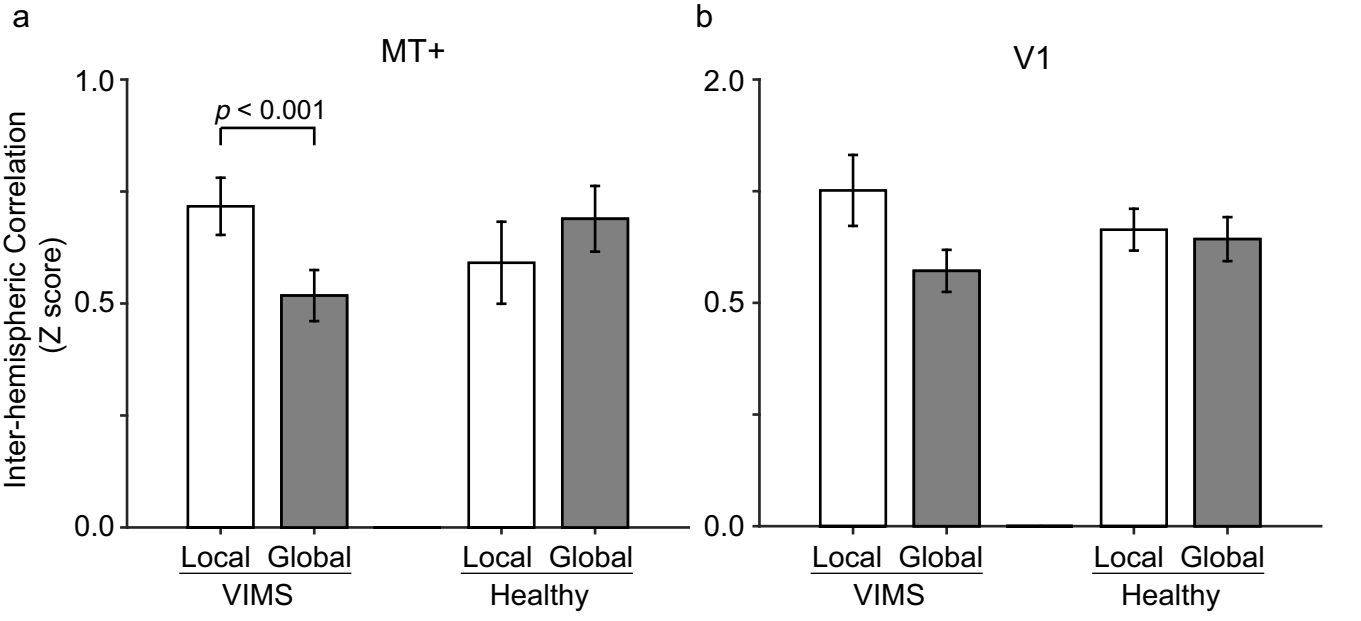

Figure 6. Average inter-hemispheric correlations between the local and global motion conditions. (a) Inter-hemispheric correlations of MT+ during the local (open bars) and the global (gray bars) conditions for the VIMS group (left) and healthy group (right). (b) Results for area V1. Error bars indicate mean ± standard error of the mean (SEM).

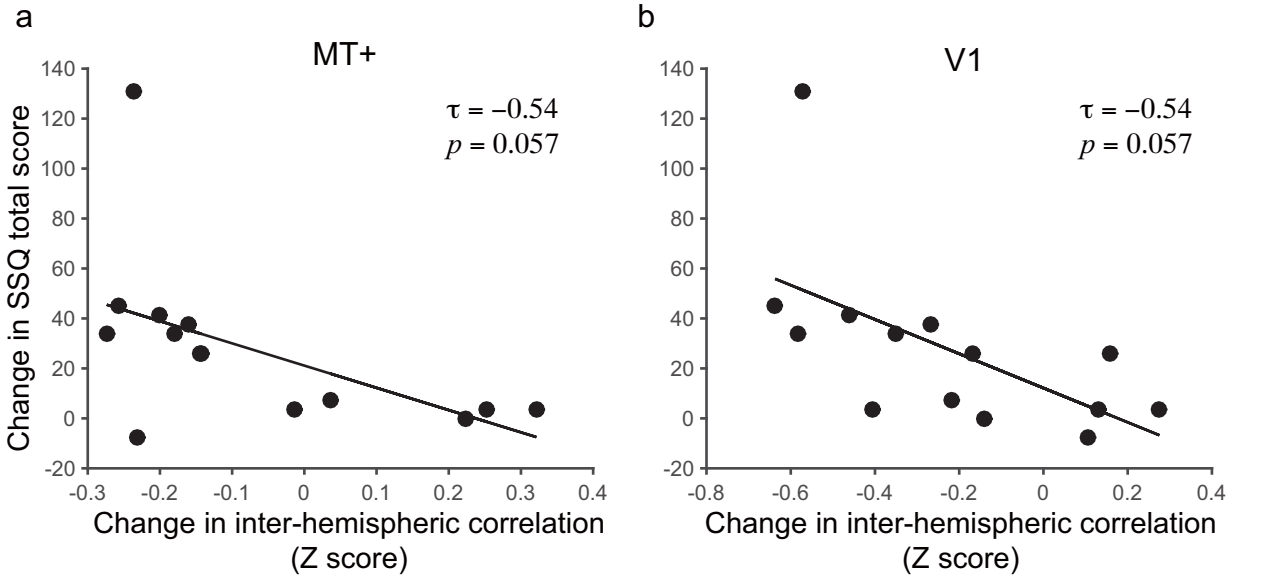

Figure 7. The relationship between inter-hemispheric correlation and SSQ score. A scatter plot of the change in inter-hemispheric correlation vs. change in SSQ total score for each subject between the local and global motion conditions (global - local). Each point represents the data of one subject (n = 14). Kendall's correlation coefficient (τ) and Bonferroni-corrected p value are shown. (a) for MT+ and (b) for V1.

Experimental Brain Research, Online Resource 3

Inter-Hemispheric Desynchronization of the Human MT+ during Visually Induced Motion Sickness

Jungo Miyazaki[1], Hiroki Yamamoto[2*], Yoshikatsu Ichimura[1], Hiroyuki Yamashiro[2], Tomokazu Murase[3], Tetsuya Yamamoto[5], Masahiro Umeda[4], Toshihiro Higuchi

[1]Frontier Research Center, Canon Inc., Tokyo, Japan

[2]Graduate School of Human and Environmental Studies, Kyoto University, Kyoto, Japan

Departments of [3]Neurosurgery and [4]Medical Informatics, Meiji University of Oriental Medicine, Kyoto, Japan

[5]Graduate School of Engineering, Kyoto University, Kyoto, Japan

E-mail: yamamoto@cv.jinkan.kyoto-u.ac.jp

Tel: +81-75-753-2978; Fax: +81-75-753-6574

Localization of visual areas based on retinotopy measurements

Visual areas, V1, V2, V3, V3A, and V7

After reconstructing each individual's cortical surface, locations of the retinotopic visual areas were identified by fMRI and standard retinotopic mapping procedures. The surface regions delimiting areas V1, V2, V3, V3A, and V7 were determined by phase-encoded retinotopic mapping methods (Engel et al.1994; Sereno et al. 1995; DeYoe et al. 1996), allowing visualization of the polar angle and eccentricity components of the retinotopic map. The retinotopic map was constructed using a phase-encoding technique where the receptive field centers were temporally coded using polar coordinates (Engel et al. 1994). The polar angle component of the map was measured by performing fMRI while the subject viewed a small wedge-shaped checkered pattern (24° center angle) that rotated counterclockwise around the fixation point, making one rotation in 60 s. The eccentricity component was measured while the subject viewed a thin checkered annulus (2° width) that expanded from the fovea to 16° peripherally over 50 s and then disappeared for 10 s. Each stimulus underwent color (black/white, red/green, or blue/yellow) pattern reversal (1 Hz) and was presented in six cycles, evoking a periodic response at a given point on the retinotopy map, where the corresponding position in the visual field was encoded in the phase of the response. The response phase for each of the polar angles or eccentricity components was computed using Fourier analysis and mapped onto the cortical surface. More details of the surface reconstruction, the retinotopy mapping, and the parcellation schema are described elsewhere (H. Yamamoto et al. 2008, 2012).

Visual area MT+

It is often difficult to localize MT+ with retinotopy measurements alone since MT+

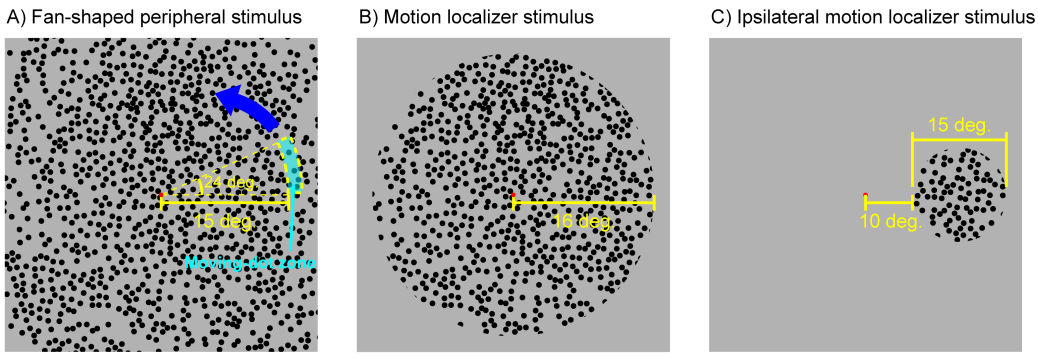

Figure S1 Visual stimuli used to localize MT and MST separately. In all stimuli, dots were 0.25° in diameter and maintained at a 15% areal density. (A) A fan-shaped phase-encoded stimulus rotating in the far peripheral visual field. The fan shape (24° center angle) was defined by moving dots on a background filled with stationary dots. Dots in the fan shape moved toward and away from fixation (8°/s), alternating direction once per second. The stimulus was rotated counterclockwise around a fixation point at 12° every 2 s (for a full rotation every 60 s) and confined in an eccentricity of 15°–16°. (B) A motion localizer stimulus. The stimulus alternated in time between moving and stationary dot fields (16° eccentricity) every 16 s and 12 times in a run. Dots moved in a way similar to those in A. (C) An ipsilateral localizer stimulus. The stimulus was positioned 10° away from a fixation point in either the left or right visual field and alternated between moving and stationary dot fields (15° diameter) every 16 s and 12 times in a run. Dots moved toward and away from the center of the field, alternating direction once per second.

has large receptive fields (RFs). This difficulty was alleviated by our small and thin phase-encoding stimuli described above. Nevertheless, there remained ambiguities and uncertainties about the exact localization. To remove this uncertainty, MT+ was carefully delineated in two steps. In the first step, MT+ was tentatively localized using the phase-encoding method described above. We noted that MT+ is presumed to include at least two sub-regions, MT and MST, the latter of which contains neurons with very large receptive fields that extend into the ipsilateral visual field (Huk et al., 2002). So, in the second step, we confirmed MT+ localization by additional measurements that allowed us to localize MT and MST separately using a new phase encoding stimulus (T. Yamamoto et al. 2009) in conjunction with an ipsilateral motion localizer (Huk et al. 2002). This confirmation step was performed for most of the subjects (12 of 14). The details of this method are described below.

In the second step, in place of a conventional rotating wedge, we used a rotating fan-shaped stimulus localized in the far peripheral visual field (Figure S1A). This new stimulus is advantageous for mapping the locations of large RFs such as those of ipsilateral-responsive neurons (IRNs) in MST because it does not stimulate central visual fields covered by the RFs of any IRNs, thereby evoking a periodic response from IRNs. This is not possible with the standard wedge that always stimulates central visual

fields. The fan shape (24° center angle) was defined by moving dots on a background filled with stationary dots (Figure S1A). The dots moved toward and away from the fixation point at a speed of 8° per second and alternated direction once per second. All dots maintained a 15% density in area. The stimulus was rotated counterclockwise about the fixation point at 12° every 2 s (1 rotation per minute, 6 rotations in a run) and confined in an eccentricity of 15°–16°.

To check the validity of the new method, we also employed two kinds of localizer experiments, one to determine motion-sensitive regions generally and the other to determine ipsilateral-responsive motion-sensitive regions. In these experiments, subjects alternately viewed dynamic and stationary dot stimuli (an eccentricity of 16 visual degrees in radius; Figure S1B). In the ipsilateral stimulation, as in Huk et al. (2002), a peripheral dot patch was presented in either the left or right visual field (Figure S1C). The 15° diameter field of dots was alternated between moving and stationary, while subjects maintained fixation on a colored point 10° from the nearest edge of the dot patch. The statistical significance and phase of fMRI activation were computed and mapped by the standard Fourier method described above.

Figure S2 and S3 show the results of these experiments for MT+ localization from two representative subjects. The results obtained with the conventional wedge stimulus are shown in Figures S2A and S3A for angular maps and Figures S2B and S3B for eccentricity maps. These maps reveal relatively clear retinotopic organization in the posterior ascending limb of the inferior temporal sulcus (ITS). It can be seen that the eccentricity maps show gradual changes from inferior to superior in this ITS region. However, the angular maps show ambiguities, particularly in the anterior part. Area MT+ was thus tentatively delineated using these maps, but with emphasis on consistency in the eccentricity representation (solid white lines in Figures S2A and S3A).

Figures S2C and S3C show the results obtained using our new phase-encoding stimulus. The new stimulus revealed clear contralateral hemifield retinotopic maps within the MT+ region. Notably, there are two mirror-symmetric angular maps in the posterior and the anterior regions, respectively, which share the upper vertical meridian (UVM) of the visual field as their border. The posterior and anterior regions are presumed to correspond to areas MT and MST, respectively. This was confirmed by the two types of motion localizers. While the general motion localizer activated the two regions together (Figures S2D and S3D), the ipsilateral localizer activated the anterior region alone (Figures S2E and S3E), as predicted from previous studies on MT and MST (e.g. Huk et al. 2002; Smith et al. 2012).

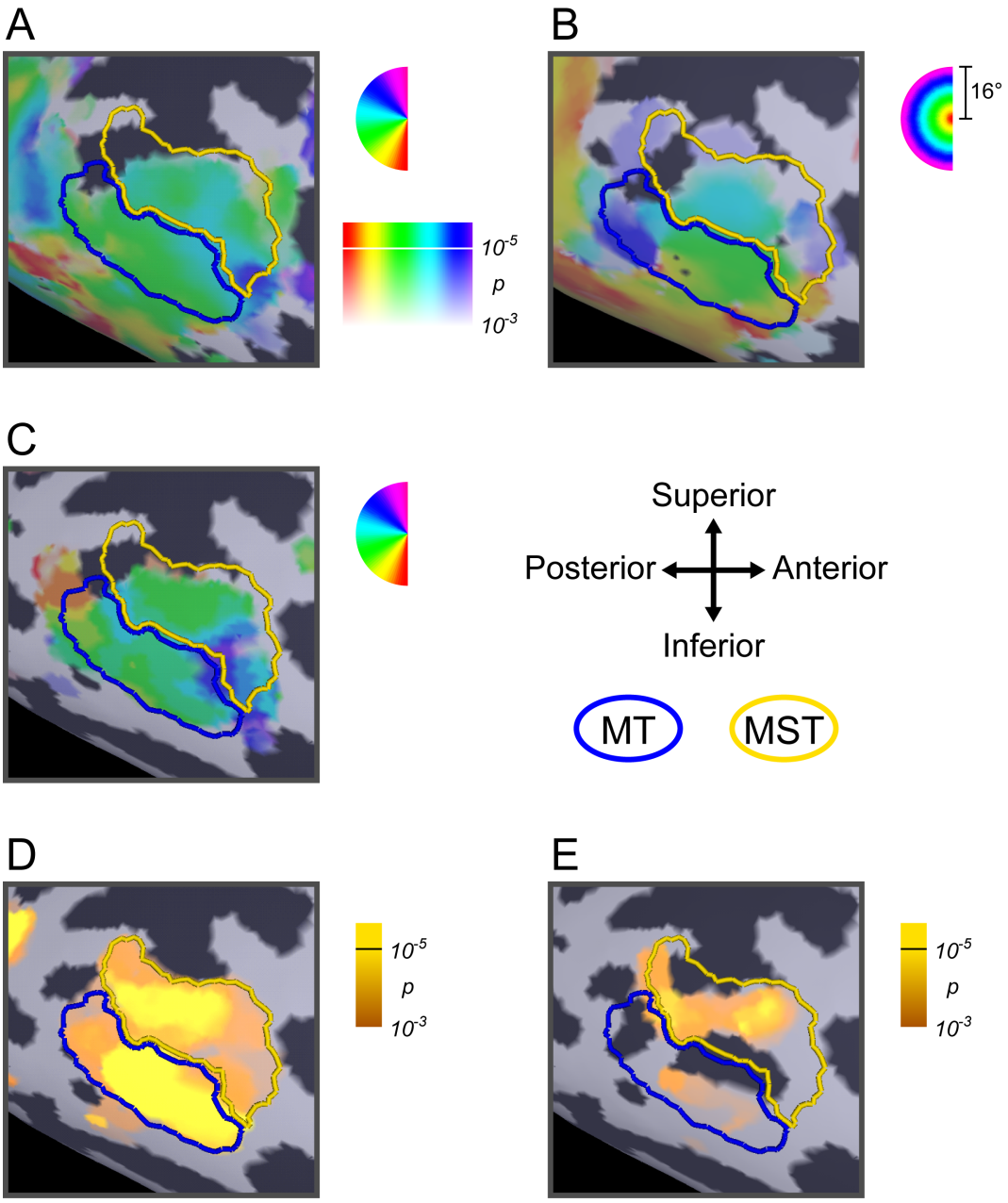

Figure S2 Locations of retinotopic areas MT and MST on the occipito-temporal cortex of a representative subject's (S1) hemisphere and their relations to retinotopic maps and loci activated by motion localizers. Areas surrounded by colored borders on inflated cortical surfaces are MT (blue) and MST (yellow). (A) Angular retinotopic maps acquired with a conventional rotating wedge stimulus. The color overlay on the cortex indicates the preferred stimulus angle at each cortical point, in accordance with the color code to the right. The more saturated the color, the higher the statistical significance of retinotopic activity, as shown in the rainbow-like color bar. (B) Eccentricity retinotopic maps acquired with a conventional expanding ring stimulus. Data are shown in the same format as in A. (C) Angular retinotopic maps acquired with a far peripheral rotating fan-shaped stimulus. (D) Motion-sensitive regions. The yellow region indicates fMRI activity evoked by a motion localizer. (E) Ipsilateral-responsive regions. The yellow region indicates fMRI activity evoked by an ipsilateral motion localizer.

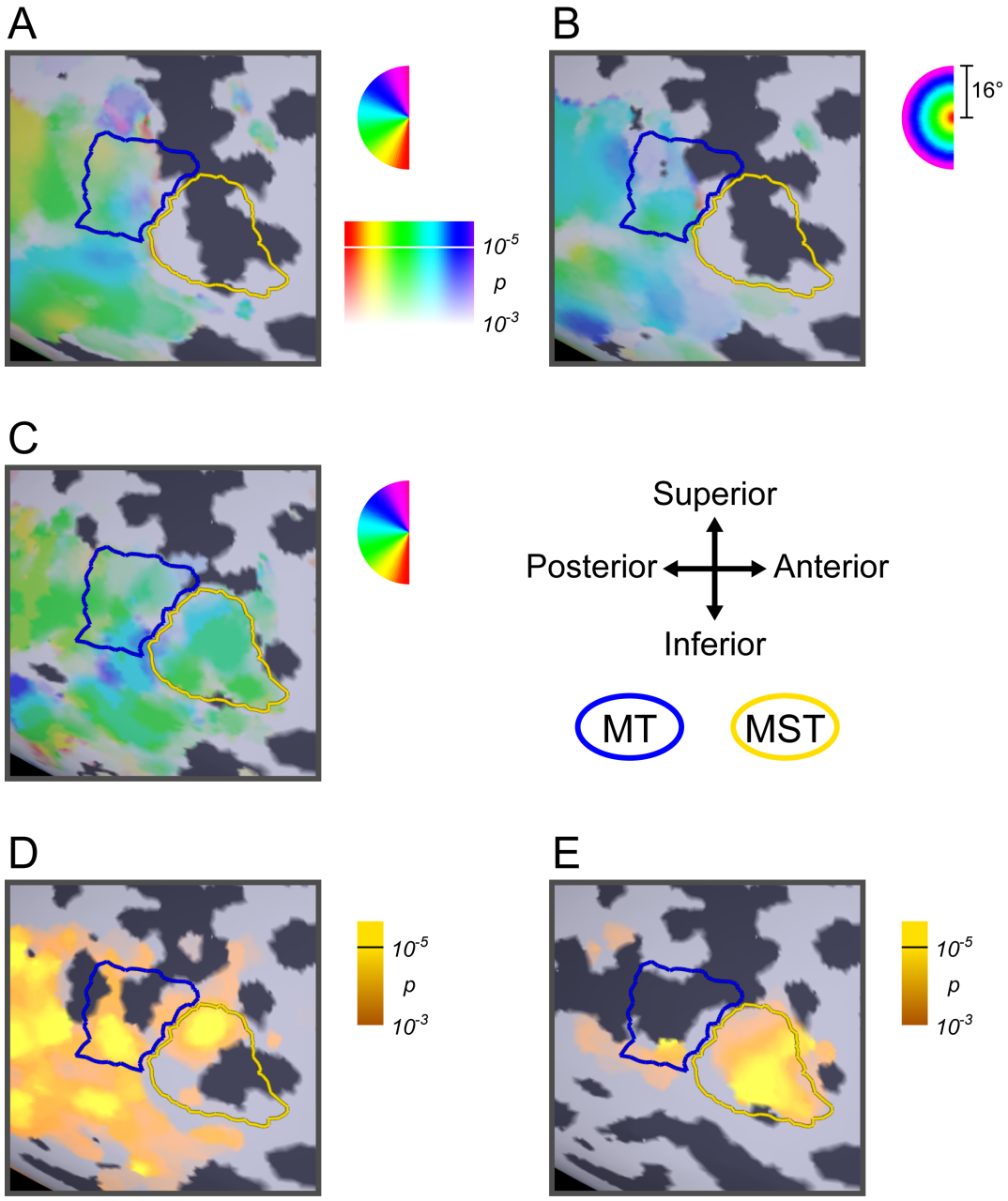

Figure S3 Locations of retinotopic areas MT and MST of another representative subject (S2) and their relations to retinotopic maps and loci activated by motion localizers, shown in the same format as in Figure S2.

References

De Yoe EA, Carman GJ, Bandettini P, Glickman S, Wieser J, Cox R, Miller D, Neitz J (1996) Mapping striate and extrastriate visual areas in human cerebral cortex. Proc Nat Acad Sci. (USA) 93: 2382-2386.

Engel SA, Rumelhart DE, Wandell BA, Lee AT, Glover GH, Chichilnisky EJ, Shadlen MN (1994) fMRI of human visual cortex. Nature 369: 525.

Huk AC, Dougherty RF, Heeger DJ (2002) Retinotopy and functional subdivision of human areas MT and MST. The Journal of Neuroscience, 22(16), 7195-7205.

Sereno MI, Dale AM, Reppas JB, Kwong KK, Belliveau JW, Brady TJ, Rosen BR, Tootell RB (1995) Borders of multiple visual areas in humans revealed by functional magnetic resonance imaging. Science 268: 889-893.

Smith AT, Wall MB, Thilo KV (2012) Vestibular inputs to human motion-sensitive visual cortex. Cerebral Cortex (New York, N.Y. : 1991), 22(5), 1068-77.

Yamamoto H, Ban H, Fukunaga M, Umeda M, Tanaka C, Ejima Y (2008) Large- and small-scale functional organization of visual field representation in the human visual cortex. In: Visual Cortex: New Research, edited by Portocello TA, Velloti RB. New York: Nova Science Publisher, 195-226.

Yamamoto H, Fukunaga M, Takahashi S, Mano H, Tanaka C, Umeda M, Ejima Y (2012) Inconsistency and uncertainty of the human visual area loci following surface-based registration: probability and entropy maps. Hum Brain Mapp 33: 121-129.

Yamamoto T, Yamamoto H, Mano H, Umeda M, Tanaka C, Kawano K (2009) A new fMRI method for subdividing the human middle temporal complex into retinotopic areas. Neuroscience Research, 65, S173.

Experimental Brain Research, Online Resource 4

Inter-Hemispheric Desynchronization of the Human MT+ during Visually Induced Motion Sickness

Jungo Miyazaki[1], Hiroki Yamamoto[2*], Yoshikatsu Ichimura[1], Hiroyuki Yamashiro[2], Tomokazu Murase[3], Tetsuya Yamamoto[5], Masahiro Umeda[4], Toshihiro Higuchi

[1]Frontier Research Center, Canon Inc., Tokyo, Japan

[2]Graduate School of Human and Environmental Studies, Kyoto University, Kyoto, Japan

Departments of [3]Neurosurgery and [4]Medical Informatics, Meiji University of Oriental Medicine, Kyoto, Japan

[5]Graduate School of Engineering, Kyoto University, Kyoto, Japan

E-mail: yamamoto@cv.jinkan.kyoto-u.ac.jp

Tel: +81-75-753-2978; Fax: +81-75-753-6574

To confirm whether the choice of cut-off frequency can affect our results, we performed analysis on the relationship between the cut-off frequency and the inter-hemispheric correlation of MT+, as well as a linear mixed-effects model analysis on the correlation data obtained for high-pass filtered fMRI signals with a 0.01-Hz cut-off. Furthermore, we conducted a simulation of the dependency of fMRI signal-to-noise ratio (SNR) on cut-off frequency.

Taken together, these analyses suggested that our findings were not meaningfully affected by the choice of cut-off frequency, and also suggested the possibility that the use of the 0.1-Hz cut-off would lead to comparable or even higher SNR in our experimental conditions. The inter-hemispheric correlation again decreased for the range of cut-off frequencies between 0.01 Hz and 0.1 Hz, and the statistical analysis using the typical 0.01-Hz cut-off again found a decrease in inter-hemispheric correlation of MT+ for only the VIMS group; however, the statistical significance did not remain after Bonferroni correction for multiple comparisons. To understand why this was the case, we performed a simulation that took account of the actual stimulus movie, the MT neurons' receptive fields, and sources of noise. The simulation showed that it would be possible to obtain an adequate, and potentially better, SNR with a 0.1-Hz cut-off. More details of these analyses are presented below.

Analysis on the relationship between cut-off frequency and decrease in inter-hemispheric correlation of MT+

As shown in Fig.S4, the inter-hemispheric correlation of MT+ was found to be

decreased for the lower cut-off frequencies than 0.1 Hz. The magnitude of the decrease was 0.16 (*mean*) ± 0.09 (*SD*), 0.12 ± 0.08, and 0.20 ± 0.05 for 0. 01 Hz, 0.032 Hz, and 0.1 Hz, respectively.

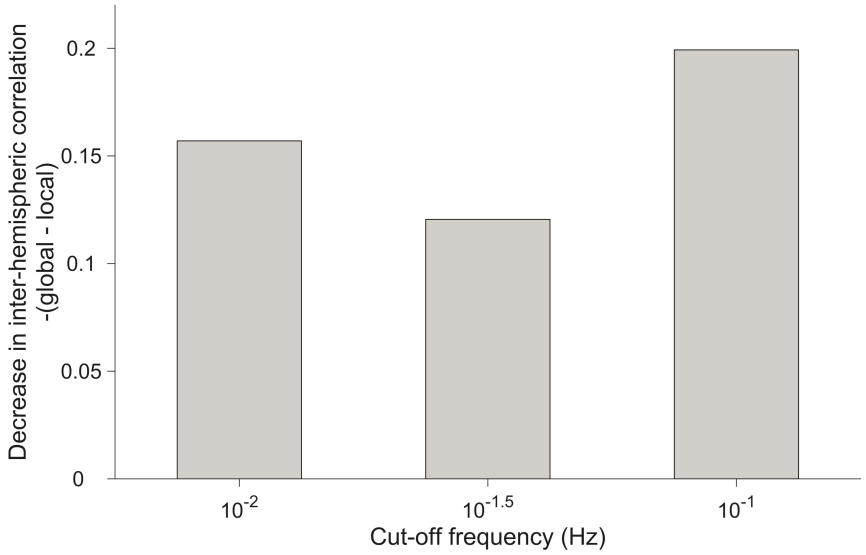

Figure S4. Decrease in inter-hemispheric correlation of MT+ for the VIMS group. The horizontal axis indicates the cut-off frequency of high-pass filtering.

Linear mixed-effects model analysis on inter-hemispheric correlations when a 0.01-Hz cut-off was used

The table S1 shows the results of statistical analysis before the Bonferroni correction for the 6 visual areas. The results were essentially similar to those obtained using the 0.1-Hz cut-off, in that the most remarkable effect of VIMS was observed for MT+. A significant CONDITION (global/local motion) × GROUP (VIMS/healthy) interaction was found only for MT+. However, the interaction was not significant after Bonferroni correction ($p = 0.168$). As evidenced by post hoc tests, the inter-hemispheric correlation of MT+ activity decreased significantly for only the VIMS group during the global motion condition, and for the other visual areas, such a VIMS-specific decrease in inter-hemispheric correlation was not observed.

Table S1 Summary statistics for linear mixed-effects model analysis on inter-hemispheric correlation when a 0.01-Hz cut-off was used

Visual area	CONDITION × GROUP interaction		Simple effect of CONDITION						Main effect of CONDITION		
	coefficient estimate ± standard error	statistics p value (χ^2)	coefficient estimate ± standard error		statistics p value (χ^2)		Effect size R^2		coefficient estimate ± standard error	statistics p value (χ^2)	Effect size R^2
			VIMS	Healthy	VIMS	Healthy	VIMS	Healthy			
MT+	−0.17 ± 0.07	.028 (4.83)	−0.17 ± 0.03	0.01 ± 0.07	.001 (11.99)	> 1 (0.03)	0.48	< 0.01	−0.09 ± 0.04	.050 (3.85)	0.13
V1	−0.02 ± 0.11	.840 (0.04)	−0.25 ± 0.07	−0.23 ± 0.05	< .001 (13.26)	.008 (8.33)	0.47	0.50	−0.24 ± 0.05	< .001 (13.02)	0.37
V2	−0.01 ± 0.09	.930 (< 0.01)	−0.13 ± 0.06	−0.12 ± 0.07	.069 (4.48)	.172 (2.95)	0.21	0.17	−0.12 ± 0.05	.015 (5.95)	0.19
V3	−0.07 ± 0.06	.260 (1.27)	−0.08 ± 0.03	−0.02 ± 0.05	.049 (5.05)	> 1 (0.18)	0.25	0.01	−0.06 ± 0.03	.075 (3.17)	0.11
V3A	0.07 ± 0.08	.425 (0.64)	0.02 ± 0.05	−0.04 ± 0.07	> 1 (0.15)	.932 (0.53)	0.01	0.03	−0.01 ± 0.04	.859 (0.03)	< 0.01
V7	−0.05 ± 0.08	.478 (0.50)	−0.07 ± 0.06	−0.02 ± 0.04	.315 (2.00)	> 1 (0.07)	0.08	0.01	−0.05 ± 0.04	.232 (1.43)	0.05

Simulation analysis of fMRI SNR

We estimated SNR as a function of cut-off frequencies by a simulation, in which the signal component was synthesized as the fMRI responses of motion-sensitive neurons to the video stimulus, using a motion-energy encoding model (Nishimoto et al. 2011), whereas noise components were synthesized as cardiac-related noise and pink (1/f) noise, with various proportions (see the Methods below for more details). The simulation showed that, as expected, the SNR with 0.1-Hz cut-off was not so bad. The SNR for a 0.1-Hz cut-off was approximately 80% on average as compared to that for 0.01-Hz cut-off (Figure S5). The simulation also showed that the higher the proportion of cardiac noise, the greater the SNR (Figure S6). This may be a reason for the somewhat pronounced effect with the 0.1-Hz cut-off.

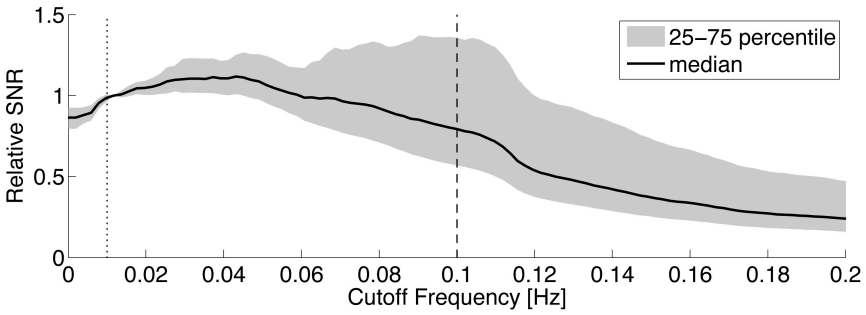

Figure S5. Relative SNR as a function of the cut-off frequency as compared to that for 0.01-Hz cut-off. The gray region shows the interquartile range (25–75th percentile, 56% and 135%, respectively, at 0.1Hz). The dashed vertical lines indicate the cut-off of 0.01 and 0.1 Hz.

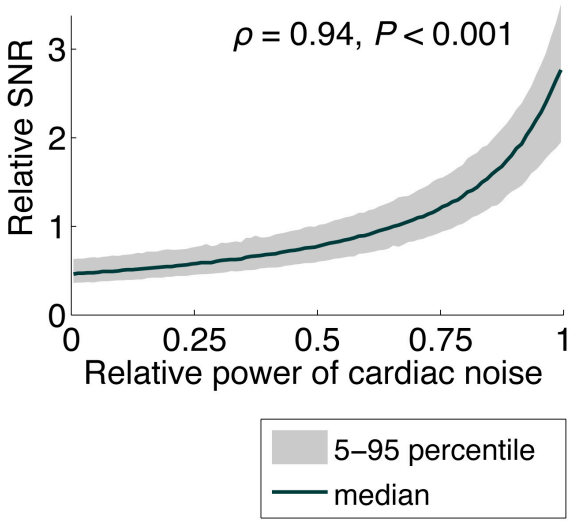

Figure S6. The relationship between the relative SNR for 0.1-Hz cut-off and the power of the cardiac noise relative to overall noise power. The black thick line indicates median SNR of 200,000 simulations, and the gray region indicates the 5th to 95th percentile range. Spearman's rank correlation coefficient (ρ) and P-value are shown.

Methods

The simulation consisted of signal generation and noise generation. Signals were generated using the video stimulus processed with motion energy filters (MEFs) (Nishimoto et al. 2011). The MEF model was a bank of 3D spatiotemporal Gabor wavelet filters, with 8 spatial frequencies (0.625, 1.25, 2.5, 5, 10, 20, 40, and 80 cycles/image), 6 temporal frequencies (0.25, 0.5, 1, 2, 4, and 8 Hz), and 8 motion directions (0°, 45°, 90°, 135°, 180°, 225°, 270°, and 315°). For simplicity, quadrature pair filters (0° and 90° phase) were used. The movie was submitted to one of the MEFs and the outputs of the quadrature pair were squared, summed, and log-transformed to generate local motion energy signals. The motion energy signal was z-transformed, clipped at 3 (i.e. 3 sigma), and convolved with hemodynamic impulse response function (HIRF) (Boynton et al. 1996), yielding local fMRI signal time-series. The fMRI signals from all of the filters were averaged in the frequency domain to obtain a signal power spectrum.

Secondly, noise composed of two components—pink noise (1/f noise) and cardiac noise—were generated. The proportions of the power of these components were randomly generated and scaled by their sum so that the sum was 1 (100 combinations for each iteration). The pink noise component was randomly generated so that the power spectral density was inversely proportional to the frequency of itself. The cardiac noise component was generated by convolving HIRF to a cardiac pulse time-course that was

randomly sampled for a continuous 360 s from those measured in two pilot experiments by pulse oximeter, each of which lasted for 840 s. Finally, the noise power spectrum was computed via the weighted average of the power spectrum of each component, which was z-transformed beforehand. This procedure was repeated 2000 times, yielding 200,000 (100 × 2000) samples.

The SNR was computed as a ratio of the power of the signal to that of the noise, where the powers for the signal and noise were the sum of the spectra above the cut-off frequency. In Figure S5, the relative SNR was calculated as the ratio of the SNR for each cut-off frequency to that for 0.01 Hz. In Figure S6, the relative SNR for 0.1-Hz cut-off is shown as a function of the relative power of cardiac noise (the ratio of the power of cardiac noise to that of overall noise). Such conversions into the relative SNR allow us to cancel out the differences in absolute powers of the signal and noise, enabling the direct comparison of SNRs for various cut-off frequencies.

References

Aguirre GK, Detre JA, Zarahn E, Alsop DC (2002) Experimental design and the relative sensitivity of BOLD and perfusion fMRI. Neuroimage 15(3) 488-500.

Boynton GM, Engel SA, Glover GH, Heeger DJ. (1996) Linear systems analysis of functional magnetic resonance imaging in human V1. J. Neurosci. 16(13) 4207-4221.

Bullmore E, Long C, Suckling J, Fadili J, Calvert G, Zelaya F, Brammer M (2001) Colored noise and computational inference in neurophysiological (fMRI) time series analysis: resampling methods in time and wavelet domains. Human brain mapping 12(2) 61-78.

Nir Y, Mukamel R, Dinstein I, Privman E, Harel M, Fisch L, Malach R (2008) Interhemispheric correlations of slow spontaneous neuronal fluctuations revealed in human sensory cortex. Nature neuroscience 11(9) 1100-1108.

Nishimoto S, Vu AT, Naselaris T, Benjamini Y, Yu B, Gallant JL (2011) Reconstructing visual experiences from brain activity evoked by natural movies. Current Biology 21(19) 1641-1646.

Experimental Brain Research, Online Resource 5

Inter-Hemispheric Desynchronization of the Human MT+ during Visually Induced Motion Sickness

Jungo Miyazaki[1], Hiroki Yamamoto[2*], Yoshikatsu Ichimura[1], Hiroyuki Yamashiro[2], Tomokazu Murase[3], Tetsuya Yamamoto[5], Masahiro Umeda[4], Toshihiro Higuchi

[1]Frontier Research Center, Canon Inc., Tokyo, Japan

[2]Graduate School of Human and Environmental Studies, Kyoto University, Kyoto, Japan

Departments of [3]Neurosurgery and [4]Medical Informatics, Meiji University of Oriental Medicine, Kyoto, Japan

[5]Graduate School of Engineering, Kyoto University, Kyoto, Japan

E-mail: yamamoto@cv.jinkan.kyoto-u.ac.jp

Tel: +81-75-753-2978; Fax: +81-75-753-6574

Results using a median-split criterion to define subject group

For more objective group division, we also employed a median-split criterion to divide subjects into VIMS and healthy groups based on the median SSQ total score. As two subjects (S7, S8 in Figure 3) had the same score, we considered the two kinds of separation and applied the mixed-effect model analysis for each case, as described below. In these new analyses, 13 of 14 subjects were placed in the same group as defined by self-report. Both analyses again showed desynchronization of MT+.

(1) In the case of changing S7 alone to the healthy group

For MT+ and V1, there was a significant CONDITION × GROUP interaction (MT+: χ^2 (1) = 9.10, p = 0.015; V1: χ^2 (1) = 10.59, p = 0.006; Bonferroni corrected). Post hoc tests for the simple effect of CONDITION showed that the inter-hemispheric correlation of MT+ and V1 activity decreased significantly in the VIMS group during the global motion condition compared to the local motion condition (MT+: $\chi^2(1) = 15.00$, $p = 0.001$; V1: $\chi^2(1) = 33.71$, $p < 0.001$, Bonferroni corrected), whereas there was no significant change in inter-hemispheric correlation of MT+ and V1 activities for the healthy group between conditions (MT+: $\chi^2(1) = 1.41$, $p > 1$; V1: $\chi^2(1) = 0.03$, $p > 1$, Bonferroni corrected). For the other visual areas V2, V3, V3A and V7, the interaction effect was not significant (V2: $\chi^2(1) = 3.76$, $p = 0.315$; V3: $\chi^2(1) = 3.71$, $p = 0.325$; V3A: $\chi^2(1) = 0.37$, $p > 1$; V7: $\chi^2(1) = 5.19$, $p = 0.136$, Bonferroni corrected) and the main effect of CONDITION was non-significant (V2: $\chi^2(1) = 5.19$, $p = 0.137$; V3: $\chi^2(1) = 1.86$, $p > 1$; V3A: $\chi^2(1) = 0.05$, $p > 1$; V7: $\chi^2(1) = 0.02$, $p > 1$, Bonferroni corrected). In sum, the results were similar to those reported in the manuscript except for V1.

(2) In the case of changing S8 alone to healthy group

For MT+, there was a significant CONDITION × GROUP interaction (χ^2 (1) = 9.15, p < 0.015, Bonferroni corrected). Post hoc tests for the simple effect of CONDITION showed that the inter-hemispheric correlation of MT+ activity decreased significantly in the VIMS group during the global motion condition compared to the local motion condition (χ^2(1) = 15.10, p = 0.001, Bonferroni corrected), whereas there was no significant change in inter-hemispheric correlation of MT+ activity for the healthy group between conditions (χ^2(1) = 1.43, p > 1, Bonferroni corrected). For the other visual areas, the interaction effect was not significant (V1: χ^2(1) = 5.43, p = 0.119; V2: χ^2(1) = 1.69, p > 1; V3: χ^2(1) = 3.65, p = 0.337; V3A: χ^2(1) = 0.38, p > 1; V7: χ^2(1) = 4.36, p = 0.221, Bonferroni corrected) and the main effect of CONDITION was non-significant (V1: χ^2(1) = 6.59, p = 0.062; V2: χ^2(1) = 5.19, p = 0.137; V3: χ^2(1) = 1.86, p > 1; V3A: χ^2(1) = 0.05, p > 1; V7: χ^2(1) = 0.02, p > 1, Bonferroni corrected). In sum, the results were similar to those reported in the manuscript.